Supporting Information

2D-C_3N_4 Encapsulated Perovskite Nanocrystals for Efficient Photo-Assisted Thermocatalytic CO_2 Reduction

*Hui Bian,[a] Deng Li,[a] Shengyao Wang,[c] Junqing Yan *[a] and Shengzhong (Frank) Liu, *[a,b]*

Experimental Section

Chemicals and gases: All chemicals including $PbBr_2$ (99.99%), CsBr (99.99%) and CH_4N_2O (99%) were purchased from Sigma-Aldrich and used without any purification.

Preparation of $CsPbBr_3$: A solid-state synthesis strategy was developed to synthesize $CsPbBr_3$. Specifically, CsBr and $PbBr_2$ were weighed at a 1:1 molar ratio (0.734 g $PbBr_2$ and 0.425 g CsBr), then placed in quartz tube and pumped vacuum for 30 minutes. After that, $CsPbBr_3$ was obtained *via* calcining quartz tube containing the mixed sample in a muffle furnace at 600 ^oC for 4 h. Besides, the reference $CsPbBr_3$ sample was prepared in the same ratio at N_2 and air condition.

Preparation of m-CN@$CsPbBr_3$ NCs: m-CN-@$CsPbBr_3$ was also fabricated *via* a solid-state reaction. Typically, the calculated $CsPbBr_3$ and urea at a mass ratio of 1:5 were mixed thoroughly and then treated by calcination in a ceramic crucible at 420 ^oC, 450 ^oC and 470 ^oC for 4 h under N_2 atmosphere, respectively. For comparison, the other two reference samples of m-CN@$CsPbBr_3$-10 and CNH@$CsPbBr_3$-3 were synthesized by same method at a mass ratio of 1:10 and 1:3, respectively. Besides, the reference m-CN sample and C_3N_4 was prepared in the same way at 450 ^oC, 480 ^oC and 550 ^oC without $CsPbBr_3$ addition, respectively.

Characterization: Transmission electron microscopy (TEM) test was performed on a FEI Tecnai G2 F20 electron microscope at an acceleration voltage of 200 kV. X-ray diffraction (XRD) patterns of all samples were obtained on a Bruker D8 Advanced diffractometer (Cu Kα1 radiation, X-ray wavelength of 1.54186 Å). Diffuse reflectance ultraviolet-visible (UV-Vis) spectra of studied samples were recorded in the air against $BaSO_4$ in the region of 200-800 nm on a Perkin-Elmer Lambda 950 spectrophotometer. X-ray photoelectron spectra (XPS) were acquired on a Kratos Axis Ultra DLD spectrometer with Al Kα ($h\upsilon$ = 1486.6 eV) as the excitation source. Steady-state Photoluminescence (PL) (excitation at 375 nm) was measured with an Edinburgh Instruments Ltd (FLS980 spectrometer) and time-resolved PL (TRPL) decay were measured with a PicoQuant FluoQuant 300. Upon the same power densities of 100 μw, Femtosecond pump-probe transient absorption (TA) measurements were

performed. All the samples were excited by the pump pulse with a wavelength of 400 nm and duration of 50 fs generated via a second harmonic generator (SHG). Then the high-speed spectrometer (HELIOS, Ultrafast Systems), where the wavelength range of the detector was in range of 400 to 850 nm, was used to detect the probe beam. XPS and UPS of the samples were carried out using a photoelectron spectrometer (ESCALAB250Xi, Thermo Fisher Scientifc), the He I light source (21.22 eV) with a bias of 5eV was used for UPS measurement. In situ FTIR tests were conducted on Nicolet IS50-IR spectrometer (Thermo Fisher, USA) equipped with a designed reaction cell and a liquid nitrogen cooled HgCdTe (MCT) detector. AutoChem1 II 2920 automated gas sorption system was utilized to assess CO_2 and CO Temperature Programmed Desorption (TPD) from 50 ^oC to 350 ^oC. The photothermal catalytic test was carried out in a miniature photothermal instrument (CEL-GPPCM-T). Steady-state surface photovoltage and transient photovoltage were massured by Surface Photovoltaic Spectroscopy (CEL-SPS1000, China Education Au-light) and Transient Photovoltage Spectrum (CEL-TPV2000, China Education Au-light). The powder samples were placed on an indium-tin-oxide (ITO) electrode, and another ITO electrode was used to press the sample into a thin film.

The calculation formula of fluorescence lifetime: The fluorescence lifetimes (τ_{ave}) are calculated using the following equation.

$$\tau_{ave} = \frac{\sum A_i \tau_i^2}{\sum A_i \tau_i} \quad (1)$$

where A_i is the decay amplitude, τ_i is the decay time.

Photo-thermo catalytic CO_2 reduction: Photo-thermo catalytic CO_2 reduction experiments were conducted in a closed circulation reactor system. The reaction temperature is gradually increased from 25 ^oC to 100^oC, 150 ^oC and 200 ^oC controlled by computer system program, respectively. A 300 W Xe-lamp was placed on the side of the heating furnace as the light source. The location of the catalysts (0.1 g) is fixed by silica wool in a quartz tube. Before the photo-thermo reaction was started, the reactor was occupied with high-purity CO_2 at a flow rate of 30 ml/min for 20 minutes in order to remove the air from the pipeline (SOXAL, 99.999%). The CO_2 gas enters the reactor at a flow rate of 5 ml/min when the heating start in a flow reactor. Besides, the catalytic CO_2 reduction of the samples were performed in a flow reactor with CO_2 and H_2O vapor as the reactants, in which condition the H_2O would continuously pass through the catalyst bed. The gaseous products at different reaction time were detected by an online gas chromatograph (GC-2014C). The photo-thermo reaction stability test is carried out by continuously increasing reaction time. The products of CO were analyzed by the gas

chromatograph equipped with a flame ionization detector (FID) and a nickel-based methanizer. The yield for CO_2 reduction products were calculated by the following equations.

$$R\ (\mu mol \cdot g^{-1} \cdot h^{-1}) = \textbf{Error!} \quad (2)$$

Where R represents the production rate of CO. c, v and $m_{cat.}$ are the detected concentration of products, the gas-flow rate and the mass of catalysts.

Using $^{13}CO_2$ as the gas source, the m-CN@$CsPbBr_3$ catalyst was tested for 13C isotopic labeling test. The gas products were collected and offline analysis was conducted using a gas chromatograph-mass spectrometry (GC-MS, Agilent 7890B GC-5977B MS) equipped with a HP-PLOT-Q-PT capillary column, respectively.

Results and Discussion

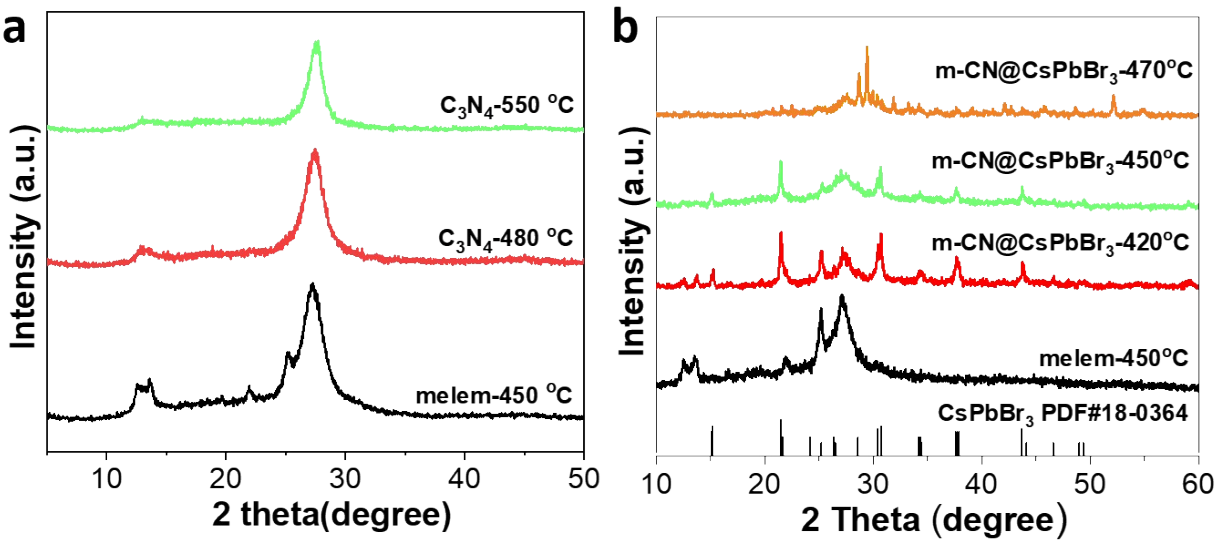

Figure S1. XRD patterns of (a) the thermal treated urea under 450 °C, 480 °C, 550 °C; (b) the thermal condensation of urea and $CsPbBr_3$ under 420 °C, 450 °C and 470 °C.

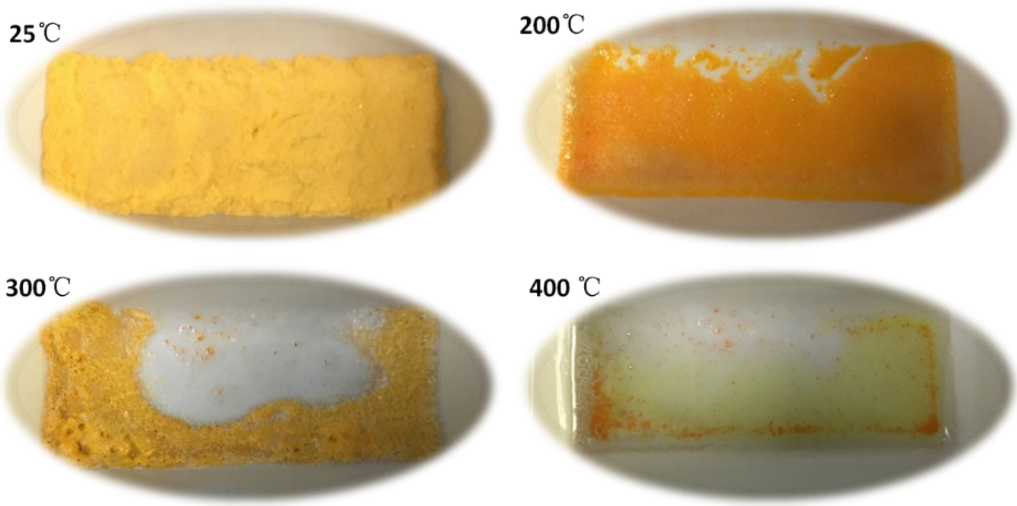

Figure S2. Photographs of the $CsPbBr_3$ and urea mixture under the different temperatures.

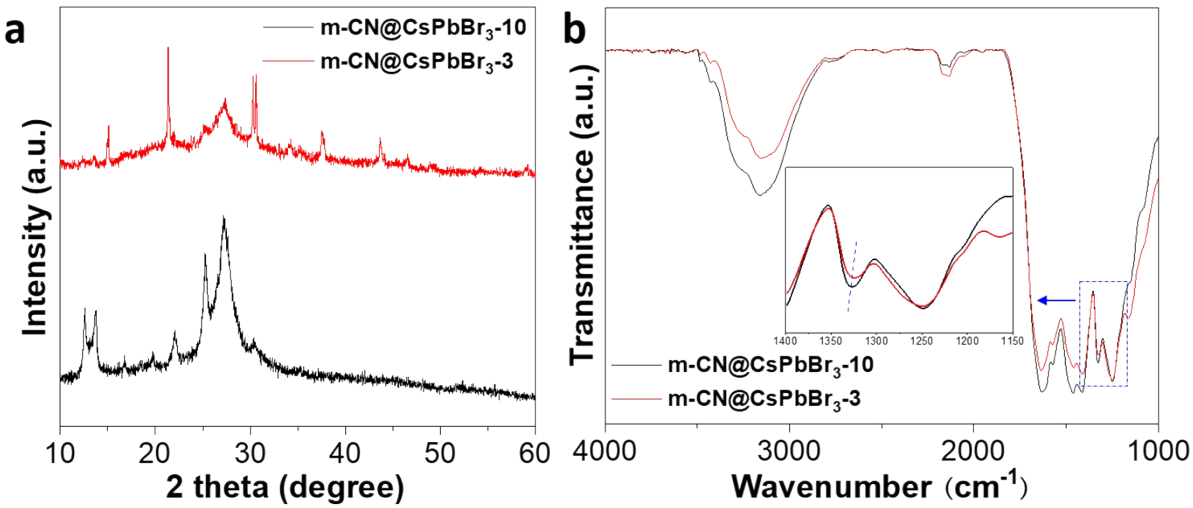

Figure S3. (a) XRD patterns and (b) FTIR results of m-CN@$CsPbBr_3$-10 and m-CN@$CsPbBr_3$-3.

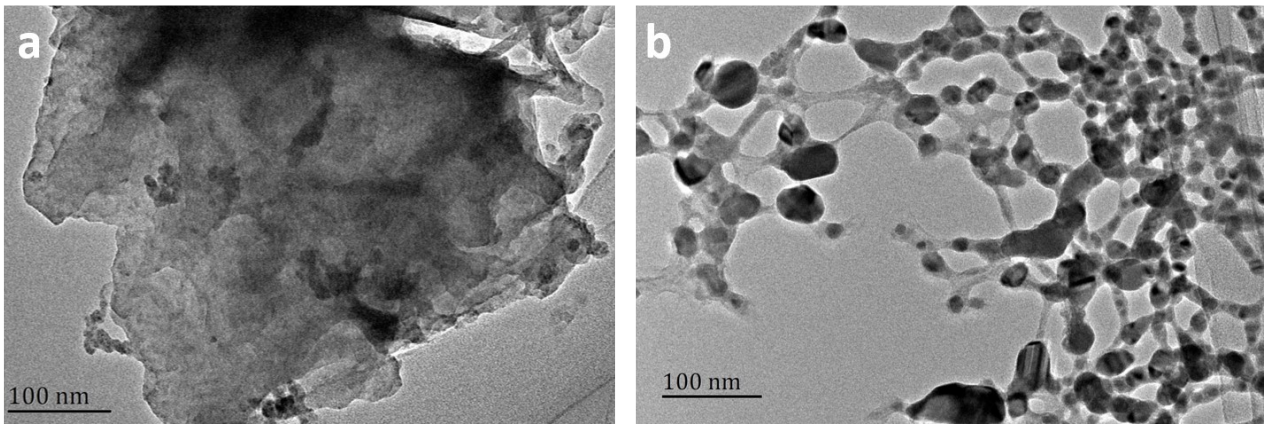

Figure S4. TEM images of (a) m-CN@$CsPbBr_3$-10 and (b) m-CN@$CsPbBr_3$-3.

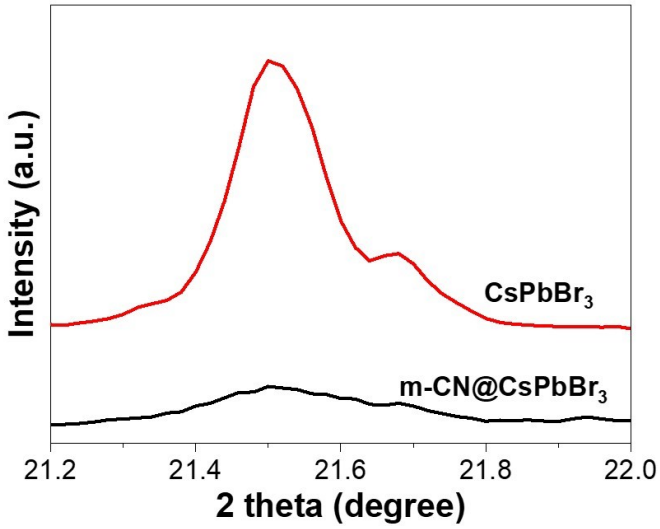

Figure S5 The magnified XRD signals of $CsPbBr_3$ and m-CN@$CsPbBr_3$ samples at the 2 theta range from 21.2 to 22 degree.

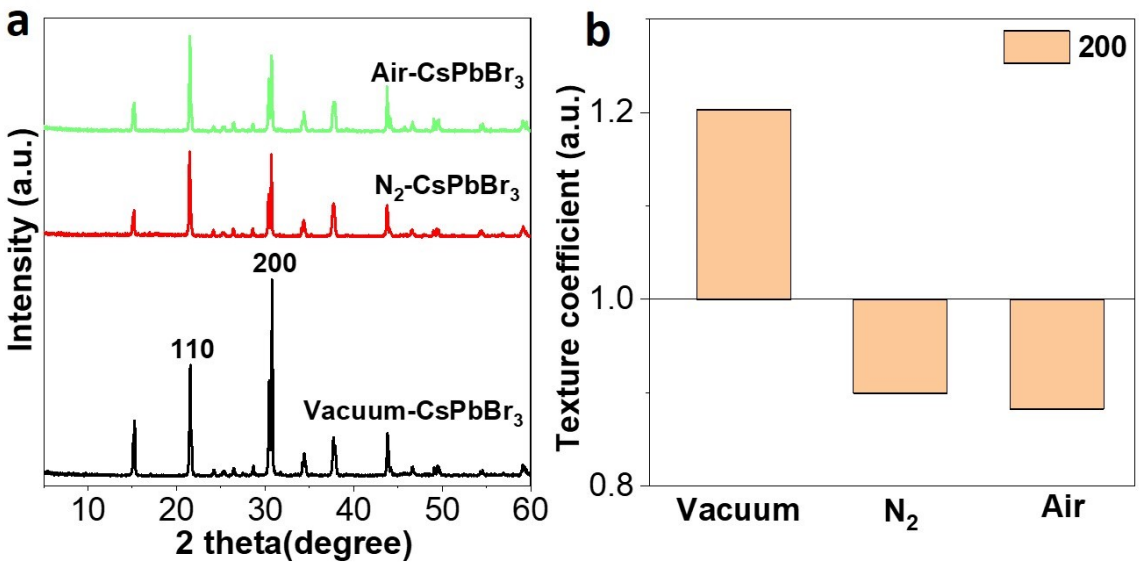

Figure S6. (a) XRD patterns of the thermal treated $CsPbBr_3$ under vacuum, N_2 and air condition; (b) Texture coefficient of [220] axis of the thermal treated $CsPbBr_3$ under vacuum, N_2 and air condition.

Calculation of the texture coefficients of $CsPbBr_3$:

The preferential of the specific crystal orientations are definite by the texture coefficient (P[hkl]). It is calculated from the result of the XRD patterns employing the following equation:

$$P[hkl]=\frac{I^{S}(hkl)*\sum I^{0}(hkl)}{I^{0}(hkl)*\sum I^{S}(hkl)} \quad (3)$$

Here, the I_S (hkl) and I_0 (hkl) are the peak intensities of the (hkl) plane in the measured XRD patterns according the standard JSPDS card of $CsPbBr_3$ (JSPDS PDF#18-0364).

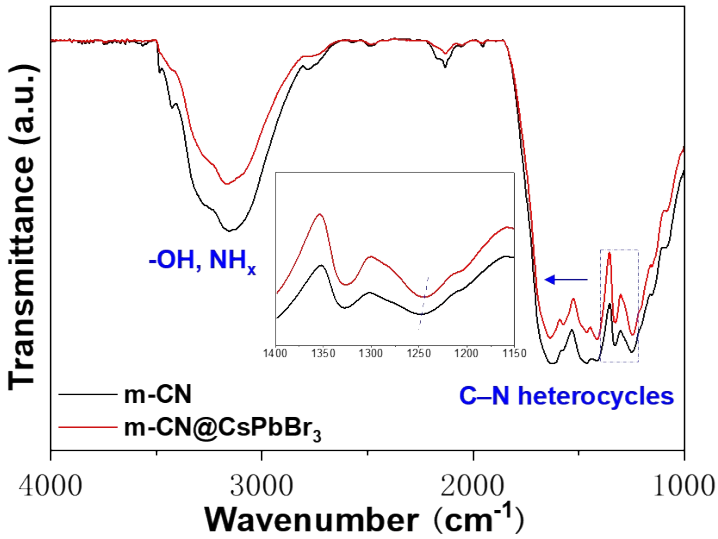

Figure S7. FTIR spectra of m-CN and m-CN@$CsPbBr_3$.

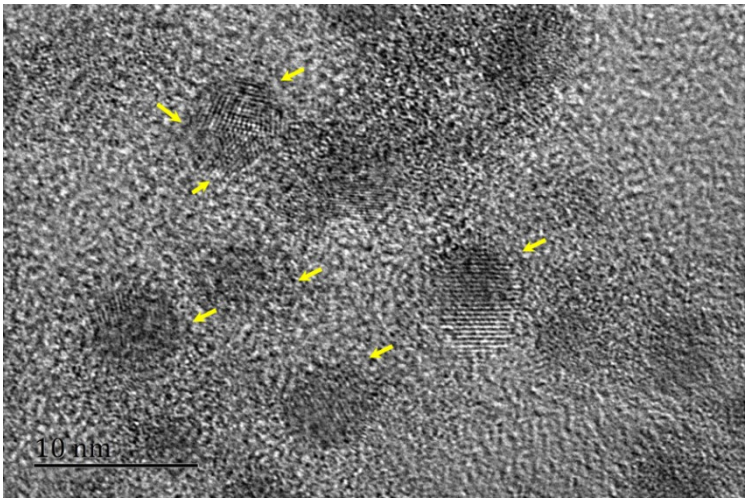

Figure S8. HRTEM result of m-CN@$CsPbBr_3$-5 sample.

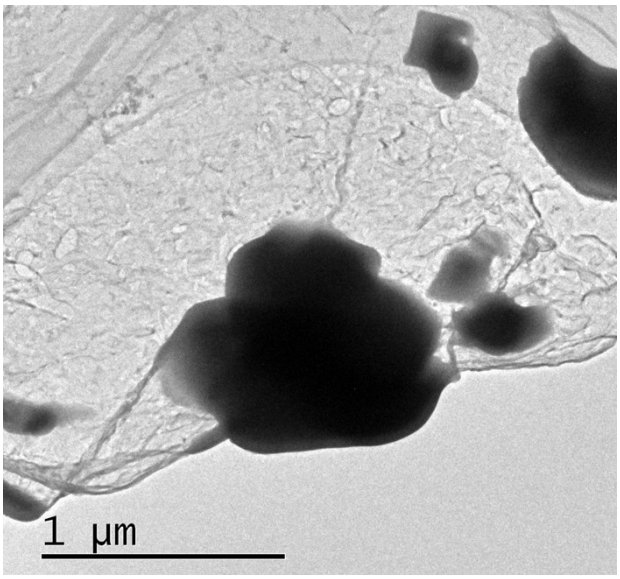

Figure S9. TEM image of $CsPbBr_3$ sample.

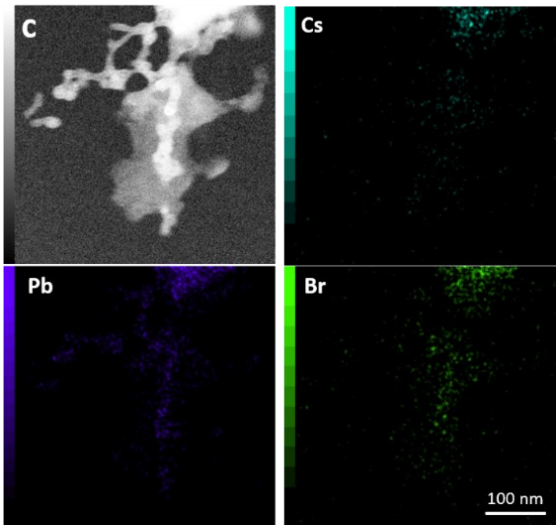

Figure S10. STEM image and the corresponding element mapping of m-CN@$CsPbBr_3$ sample.

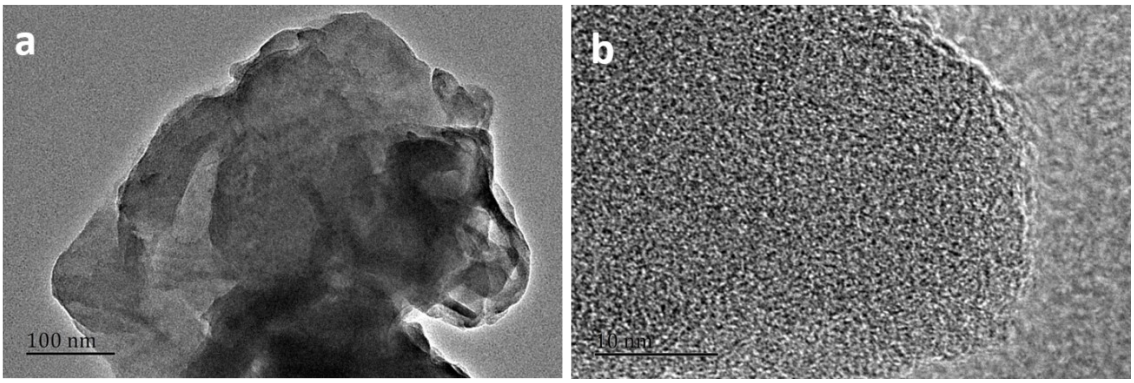

Figure S11. (a) TEM and (b) HRTEM images of the reference m-CN sample.

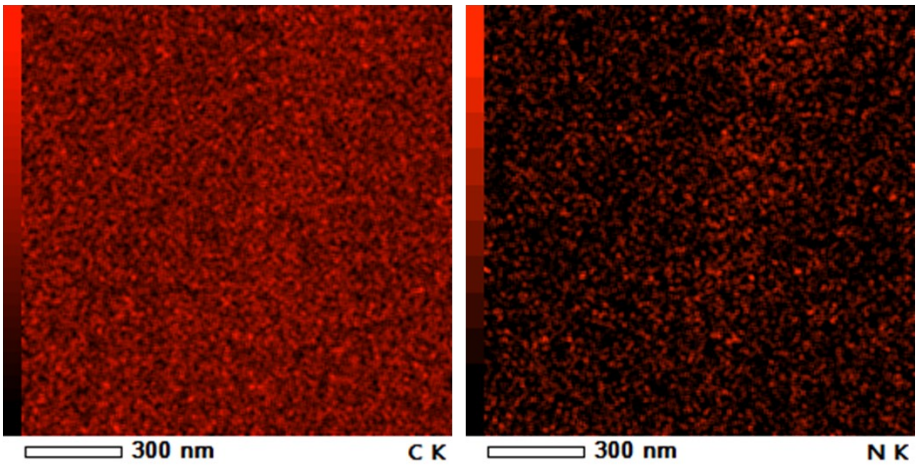

Figure S12. The element mapping results of element C and N of the sample of m-CN@$CsPbBr_3$.

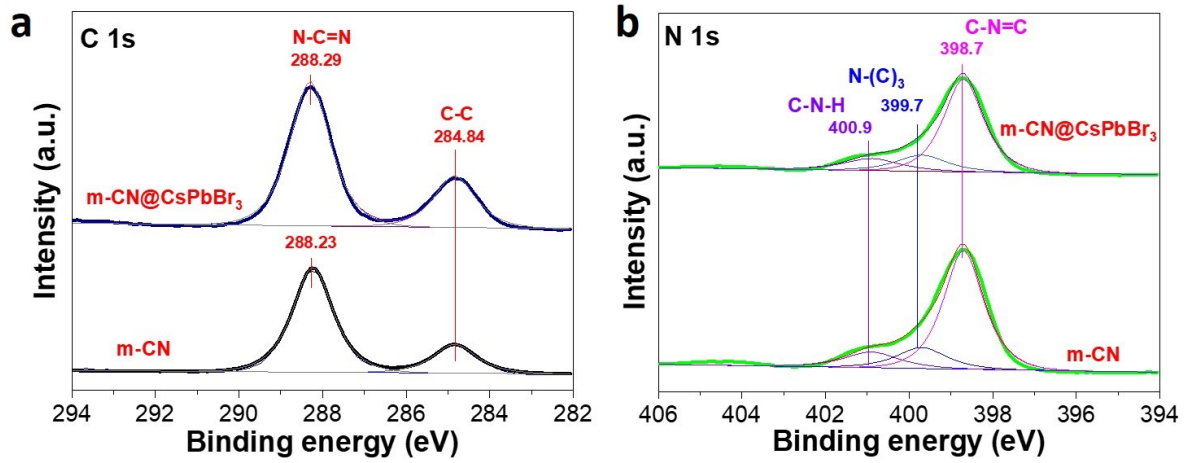

Figure S13. XPS curves of (a) C 1s and (b) N 1s of the samples of m-CN and m-CN@$CsPbBr_3$.

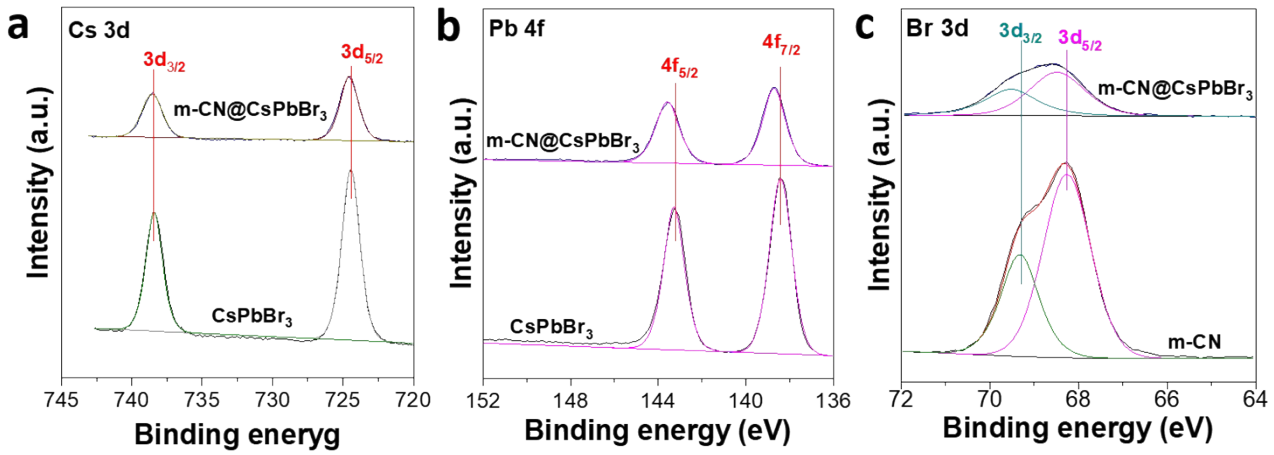

Figure S14. XPS curves of (a) Cs 3d, (b) Pb 4f and (c) Br 3d of the samples of $CsPbBr_3$ and m-CN@$CsPbBr_3$.

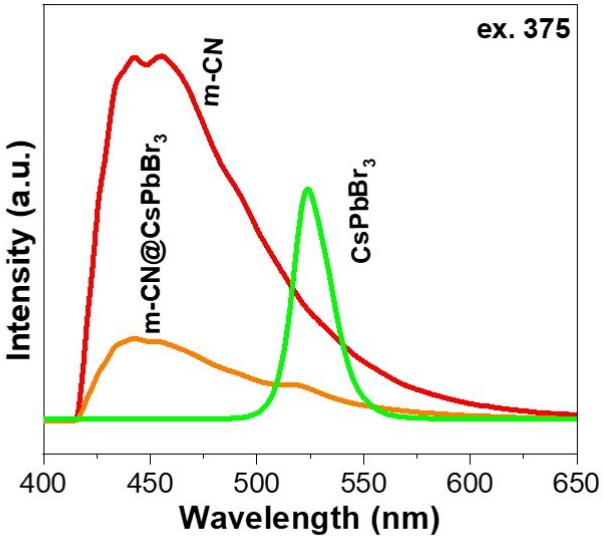

Figure S15. PL results of the samples of m-CN, $CsPbBr_3$ and m-CN@$CsPbBr_3$.

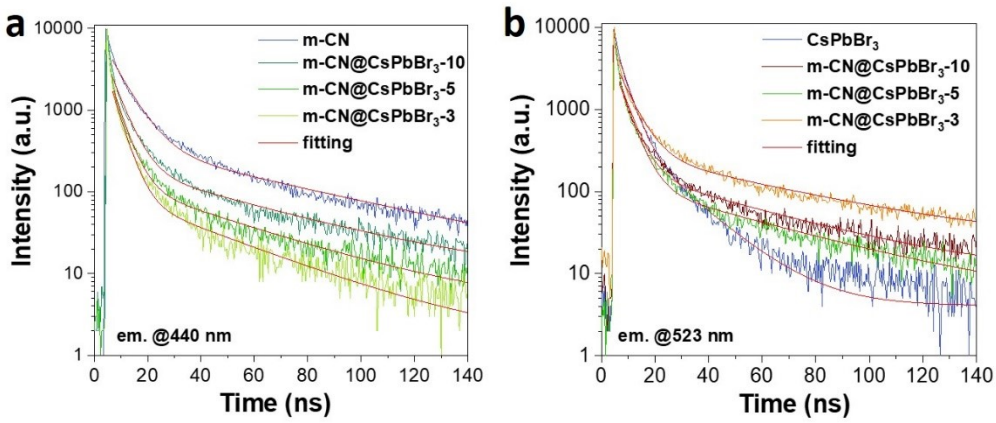

Figure S16. The transient PL results of the m-CN, $CsPbBr_3$ and m-CN@$CsPbBr_3$ samples, (a) emission 440 nm and (b) 523 nm.

Table S1. The corresponding fitting results at emission of 440 nm based on Figure S16a.

Sample	τ_{ave} (ns)	τ_1 (ns)	amplitude τ_1 (%)	τ_2 (ns)	amplitude τ_2 (%)
m-CN	28.84	55.82	45.02	6.75	54.98
m-CN@$CsPbBr_3$-10	22.73	45.35	44.2	4.82	55.80
m-CN@$CsPbBr_3$-5	14.16	34.53	33.62	3.84	66.38
m-CN@$CsPbBr_3$-3	18.11	39.01	40.16	4.08	59.84

Table S2. The corresponding fitting results at emission of 523 nm based on Figure S16b.

Sample	τ_{ave} (ns)	τ_1 (ns)	amplitude τ_1 (%)	τ_2 (ns)	amplitude τ_2 (%)
$CsPbBr_3$	7.78	15.47	33.78	3.86	66.22
m-CN@$CsPbBr_3$-10	22.57	43.95	45.91	4.42	54.09
m-CN@$CsPbBr_3$-5	30.09	52.67	52.15	5.48	47.85
m-CN@$CsPbBr_3$-3	20.80	45.55	39.84	4.41	60.16

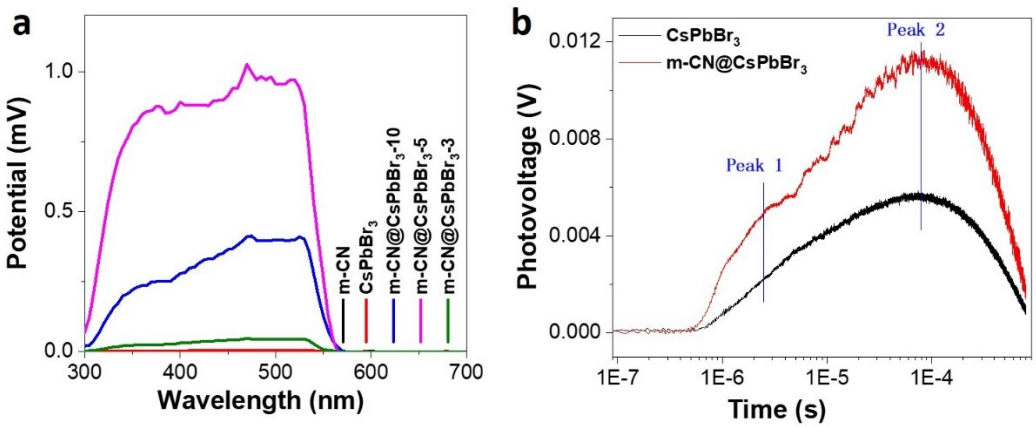

Figure S17. (a) Surface photovoltage plots of the m-CN, $CsPbBr_3$ and m-CN@$CsPbBr_3$ samples. (b) Transient photovoltage spectrum of $CsPbBr_3$ and m-CN@$CsPbBr_3$.

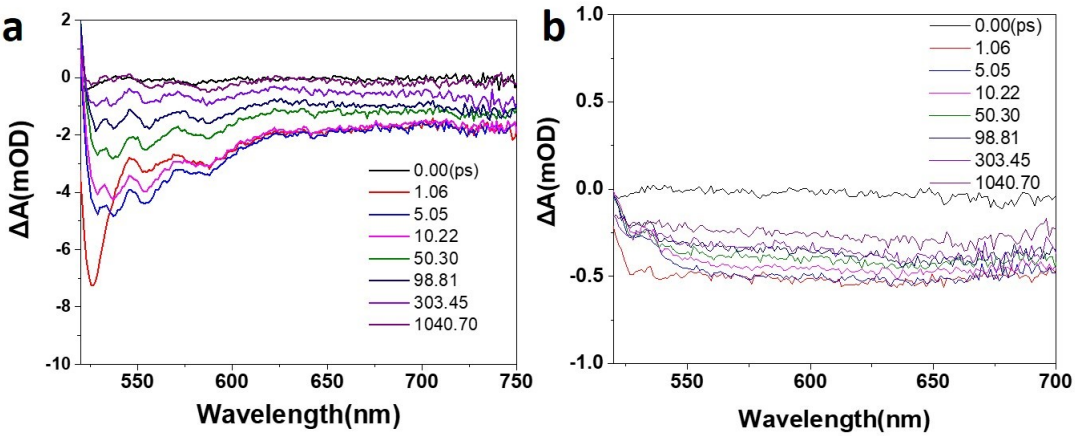

Figure S18. Transient absorption spectroscopy of (a) $CsPbBr_3$ and (b) m-CN@$CsPbBr_3$.

Table S3. The corresponding fitted lifetimes of $CsPbBr_3$ and m-CN@$CsPbBr_3$ based on Figure 2c.

Sample	τ_{ave} (ps)	τ_1 (ps)	amplitude τ_1 (%)	τ_2 (ps)	amplitude τ_2 (%)
$CsPbBr_3$	77.16	20.98	12.97	80.98	56.54
m-CN@$CsPbBr_3$-5	197.71	28.31	18.70	216.26	23.63

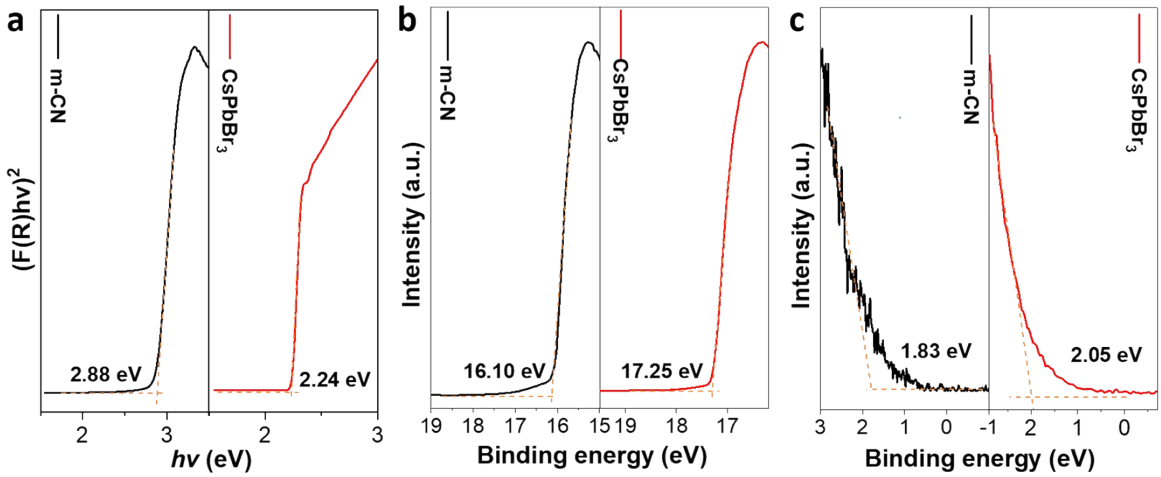

Figure S19. (a) Tauc plot of m-CN and $CsPbBr_3$ derived from the UV-vis spectra; (b) and (c) UPS spectra of m-CN and $CsPbBr_3$ test under UV light at target current of 50 mA and bias of 5 eV.

Table S4. The corresponding E_f, E_v and E_c calculation results based on Figure S19.

Sample	Eg (eV)	Emax (eV)	Emin (eV)	E_{VBM} (eV/Vvs RHE)	E_{CBM} (eV/Vvs RHE)	E_f (eV/Vvs RHE)
m-CN	2.88	16.10	1.83	-6.95/+2.45	-4.07/-0.43	-5.12/0.62
$CsPbBr_3$	2.24	17.25	2.05	-6.02/+1.52	-3.58/-0.92	-3.97/-0.53

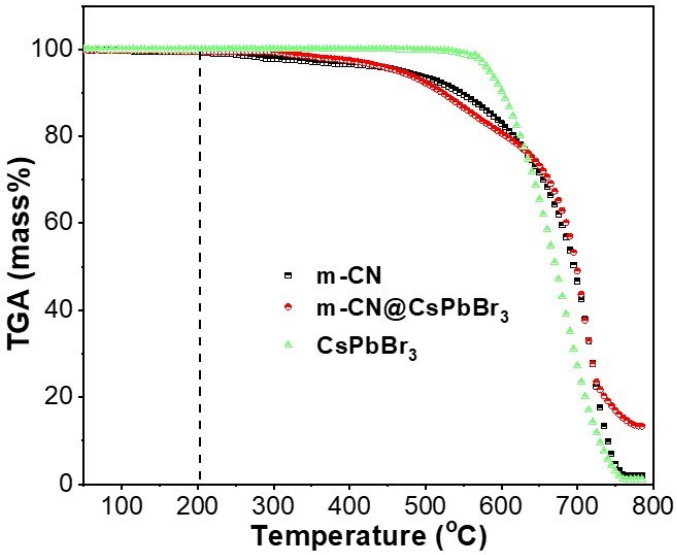

Figure S20. TGA curves of the m-CN, $CsPbBr_3$ and m-CN@$CsPbBr_3$ samples.

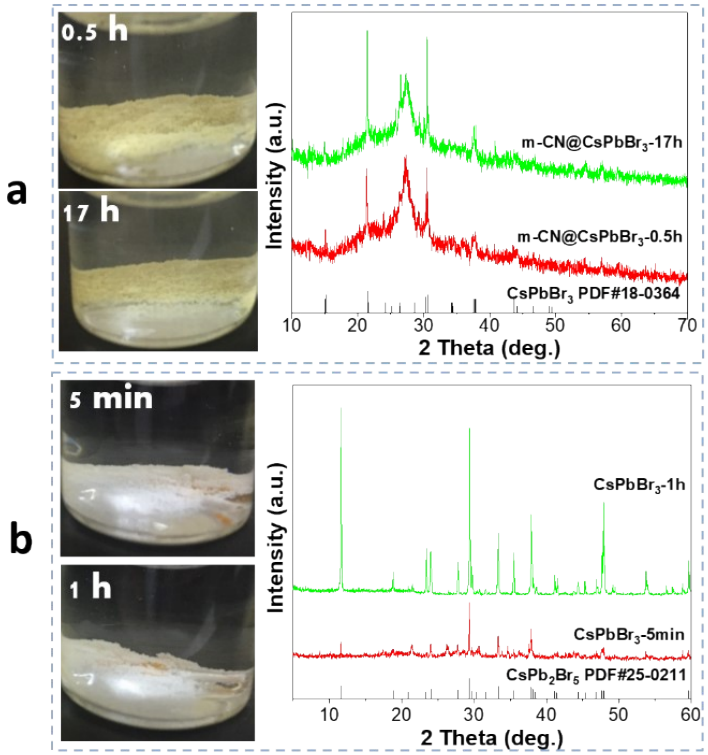

Figure S21. Photographs and the corresponding XRD patterns of (a) the m-CN@$CsPbBr_3$ sample after being placed in water for 0.5 and 17 h; (b) the reference $CsPbBr_3$ sample after being placed in water for 5min and 1 h.

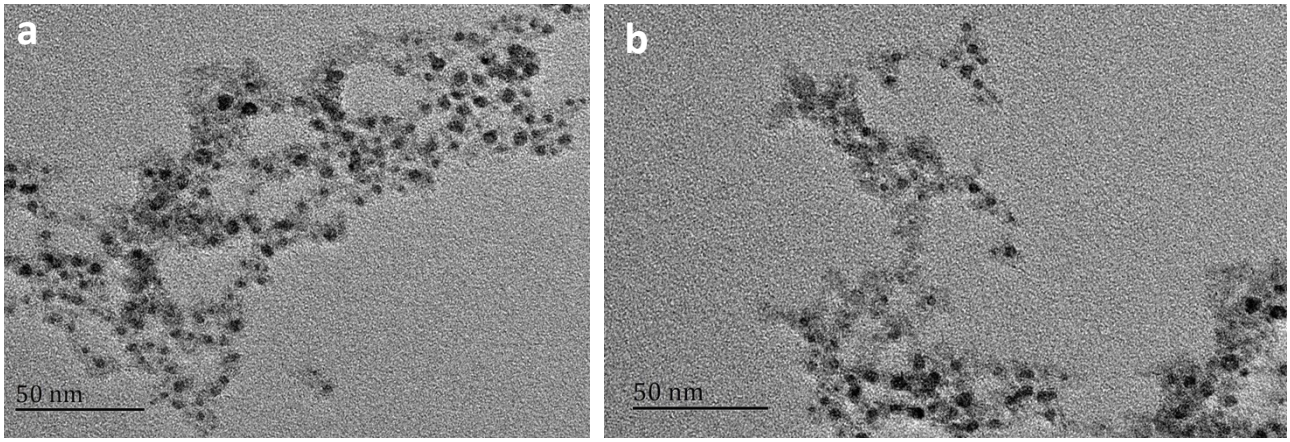

Figure S22. TEM images of m-CN@$CsPbBr_3$ sample after placing in water (a) 0.5 h and (b) 17 h.

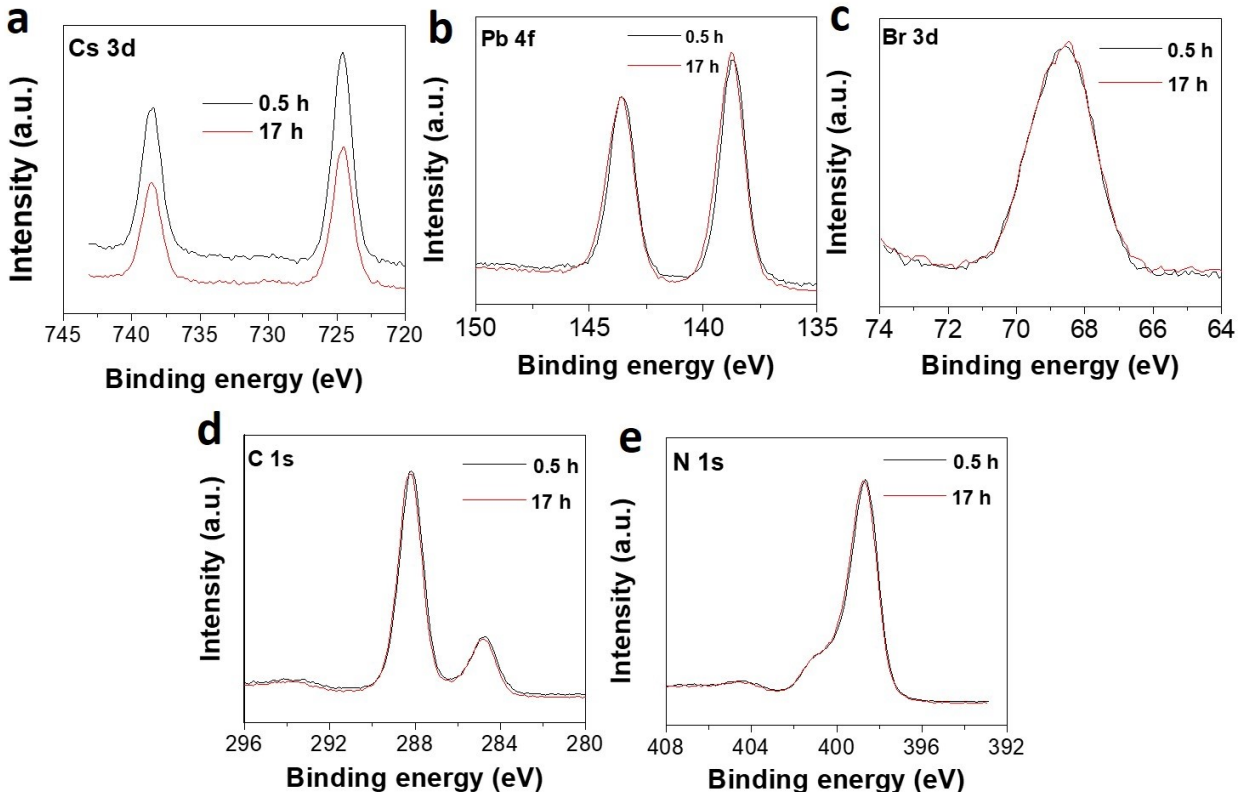

Figure S23. XPS curves of (a) Cs 3d, (b) Pb 4f, (c) Br 3d, (d) C 1s and (e) N 1s of m-CN@$CsPbBr_3$ treated in water 0.5 and 17h.

Table S5. A summary of the photocatalytic and Photo-Thermocatalytic CO_2 reduction performances in condition of H_2O and CO_2.

Catalyst	Co-catalyst	conversion rate μmol g^{-1} h^{-1}		Light source	Main product selectivity (%)	Condition	References
		CH_4	CO				
$Cs_3Bi_2Br_9$	-	-	26.9	AM 1.5G	98. 7	CO_2/H_2O vapor	[1]
$CsPbBr_3$@ZIF-67(1,4)	-	3.51	0.77	100W Xe lamp		CO_2/H_2O vapor	[2]
$CsPbBr_3$/BZNW/MRGO	-	6.29	0.85	150 W Xe lamp	≈96.7	CO_2/H_2O vapor	[3]
$CsPbBr_3/C_3N_4$	-	-	148.9	Xe lamp, ≥ 420 nm	71.4	acetonitrile / water	[4]
Cubic $NaNbO_3$	1 wt % Pt	4.86	-	Xe lamp, > 300 nm	1.5	CO_2/H_2O vapor	[5]
$CsPbBr_3$@GO	-	2.5	4.9	AM 1.5G	66.4	ethyl acetate	[6]
$CsPbBr_3$ NC/a-TiO_2	-	6.72	3.9	AM 1.5G	83.3	CO_2 and ethyl acetate	[7]
$Cs_2AgBiBr_6$ NCs		1.6	2.35	AM 1.5G, 100 mW/cm^2		ethyl acetate	[8]
$TiO_2/CsPbBr_3$	-	-	9.02	300 W Xe arc lamp	-	Acetonitrile and H_2O	[9]
Zn/Ti LDH	-	3.77	-	Hg lamps (185 nm, 4 W and 254 nm, 8 W)	-	CO_2/H_2O vapor	[10]
a-Fe_2O_3/ Amine-RGO/$CsPbBr_3$	-	12.1	-	AM1.5G and 420nm optical filte	93.4	CO_2/H_2O vapor	[11]
(Pt/TiO_2)@rGO	0.8–0.9 wt% Pt	41.3		Xe lamp (320–780 nm)	99.1	CO_2/H_2O vapor	[12]
TiO_{2-x}	-	1.63	-	Xe lamp, AM 1.5 filter	85.8	CO_2/H_2O vapor	[13]
m-CN@$CsPbBr_3$	-	-	42.8	A 300 W Xe lamp	88.8	CO_2/H_2O vapor	This Work

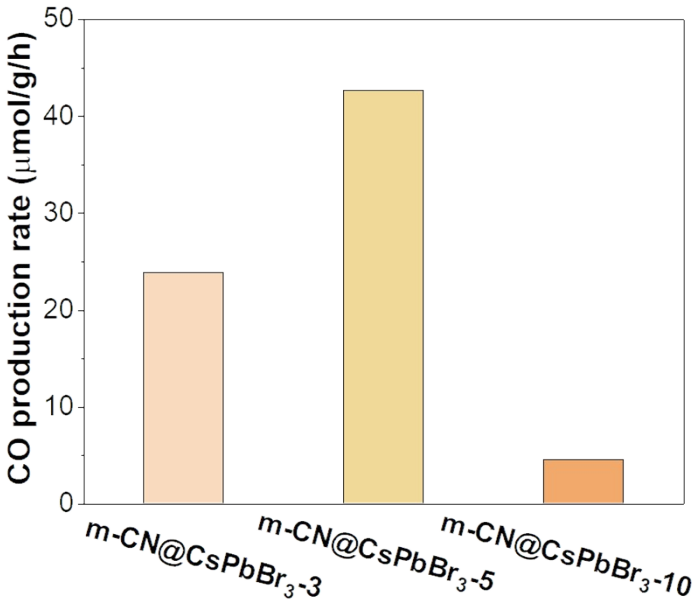

Figure S24. The catalytic activity of CO_2 conversation to CO for m-CN@$CsPbBr_3$ by changing the m-CN and $CsPbBr_3$ ratios at 150 °C and 3 suns.

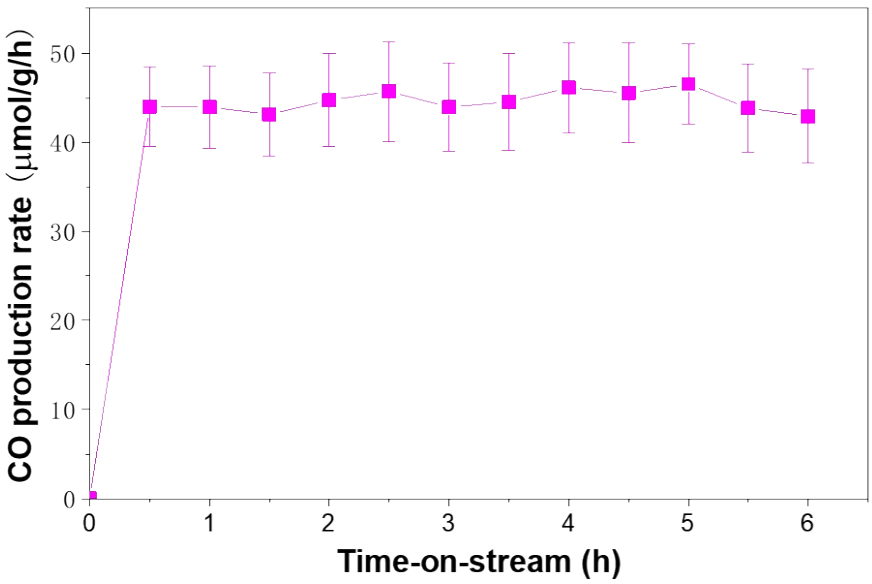

Figure S25. The CO_2 reduction to CO performance of m-CN@$CsPbBr_3$-5 samples under the temperature of 150 °C and 3 suns.

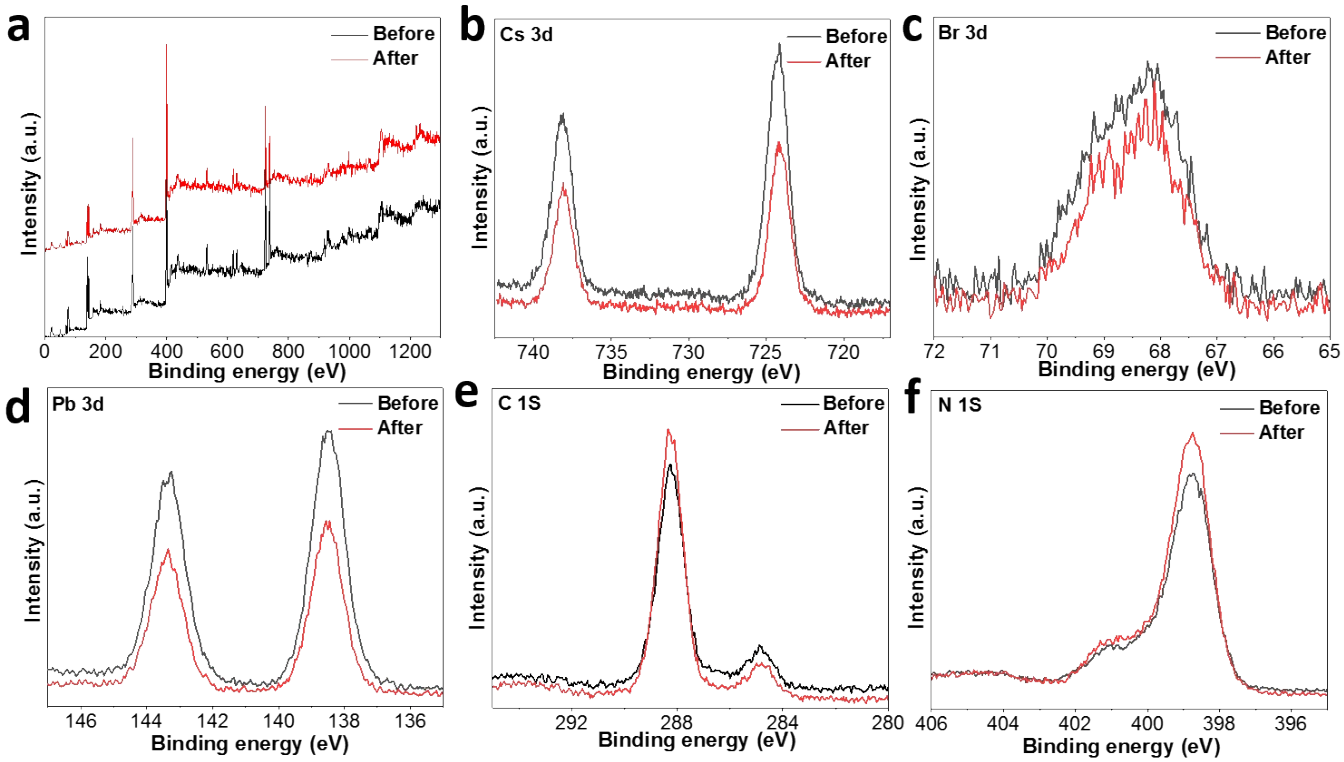

Figure S26. XPS spectra of (a) full spectrum; (b) Cs 3d, (c) Pb 4f, (d) Br 3d, (e) C 1s and (f) N 1s of m-CN@$CsPbBr_3$-5 before and after photo-thermocatalytic test.

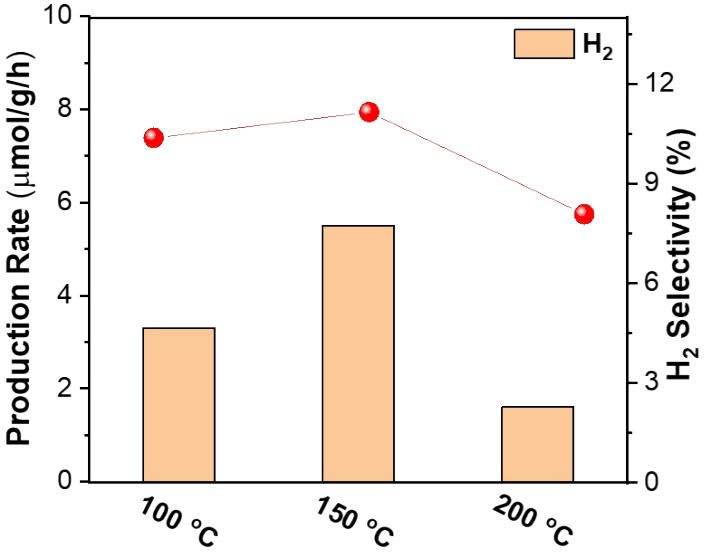

Figure S27. Production rate and selectivity of H_2 for photo-thermo catalytic CO_2 reaction on m-CN@$CsPbBr_3$ catalysts at 100 °C, 150 °C and 200 °C. The selectivity of H_2 were calculated by the following equation.

$$\mathrm{H_2\ Selectivity\ (\%)} = \frac{R_{H2} * 2}{R_{CO} * 2 + R_{H2} * 2} \tag{4}$$

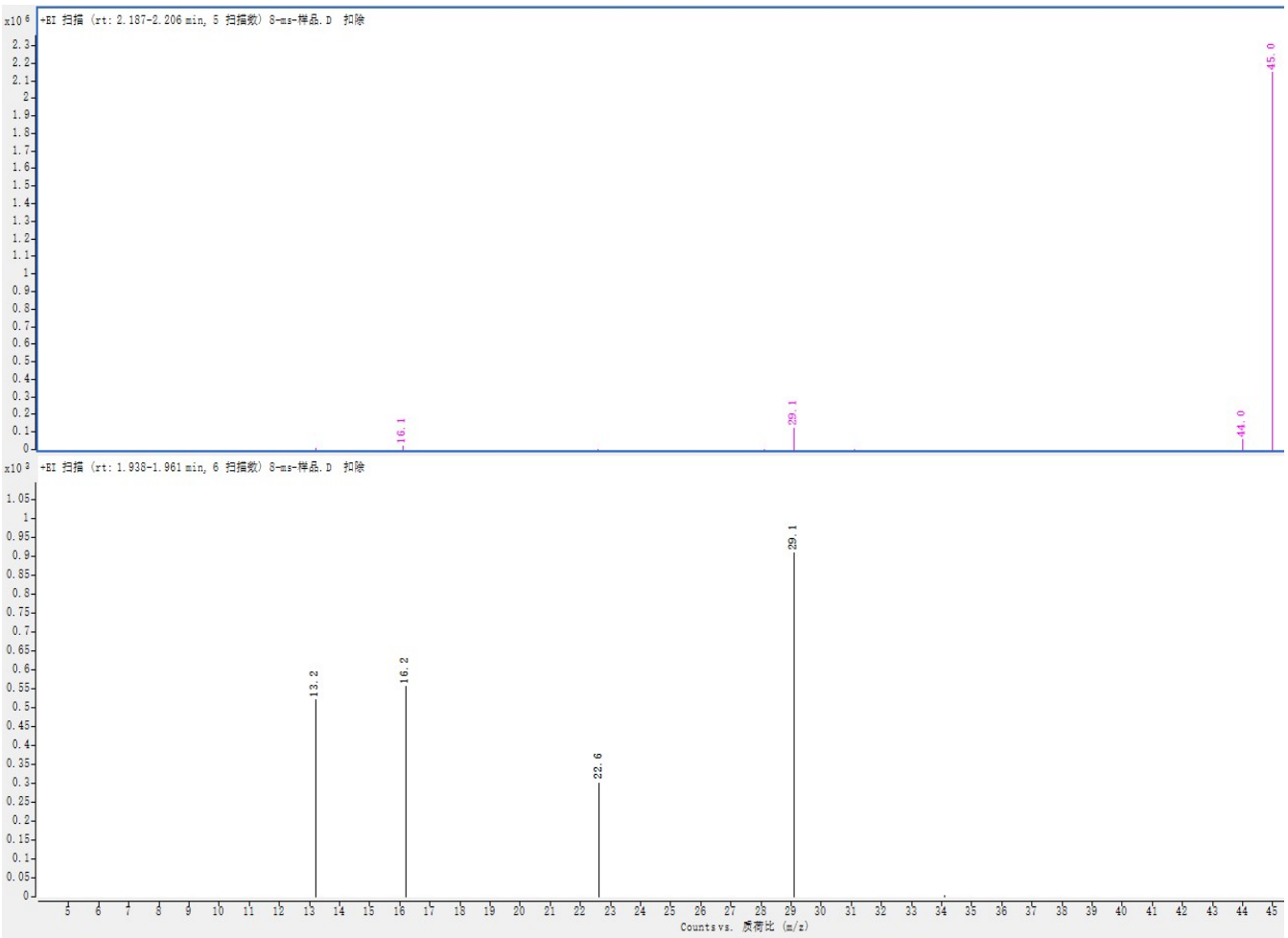

Figure S28. The screen shots of MS result of ^{13}CO produced over m-CN@$CsPbBr_3$ from the $^{13}CO_2$ isotope experiment under thermocatalysis.

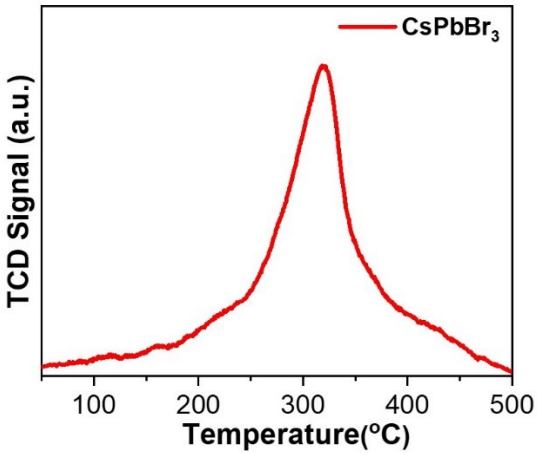

Figure S29. CO_2-TPD result of $CsPbBr_3$ sample.

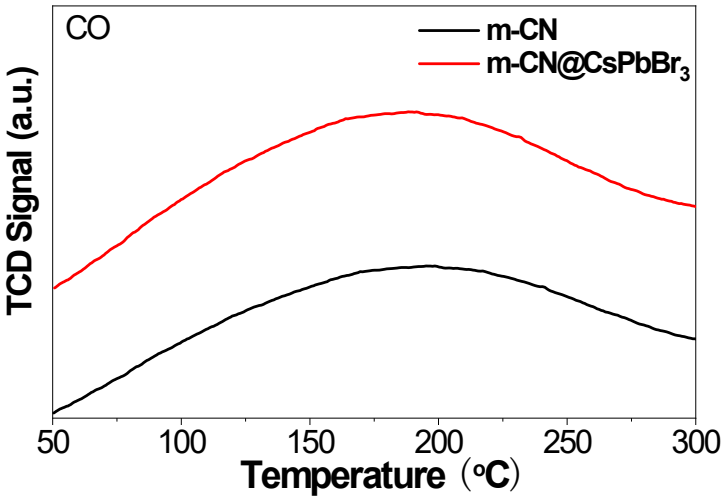

Figure S30. CO-TPD results of m-CN and m-CN@$CsPbBr_3$ samples.

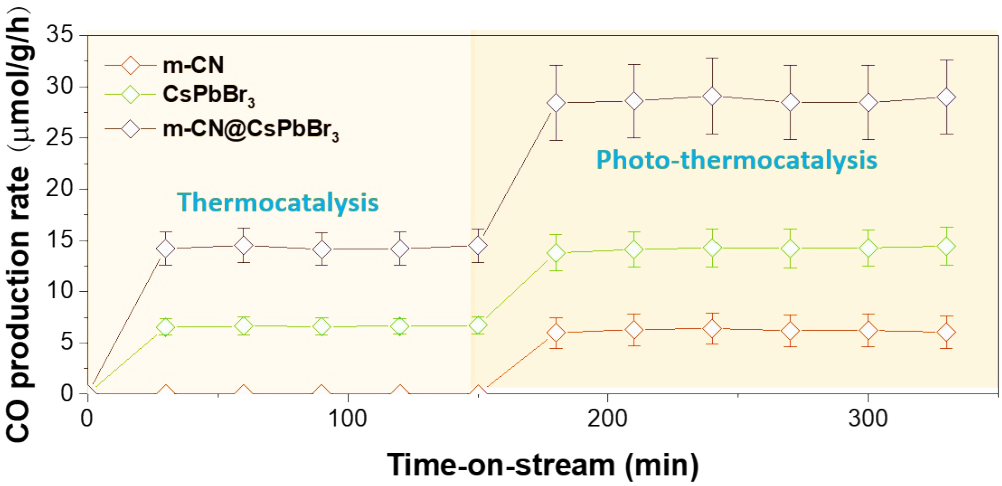

Figure S31. The thermocatalytic and photo-thermocatalytic results of m-CN, $CsPbBr_3$ and m-CN@$CsPbBr_3$ samples under the temperature of 100 °C.

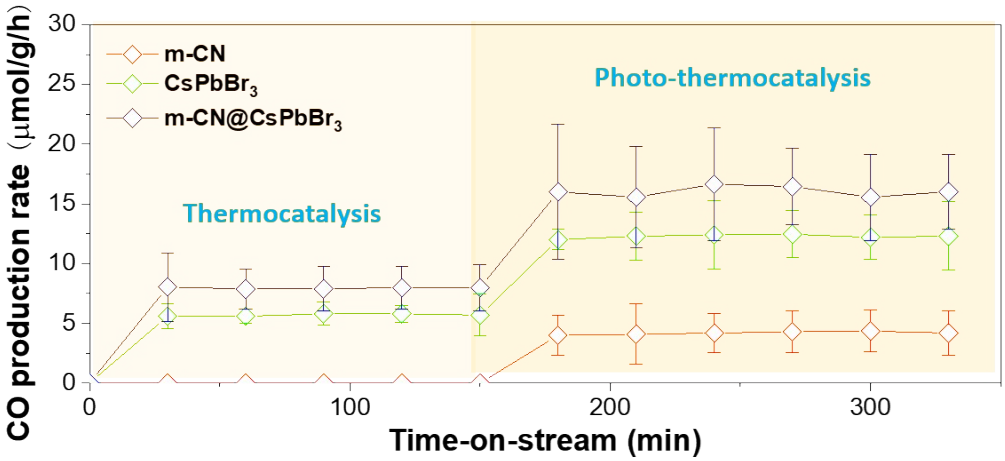

Figure S32. The thermocatalytic and photo-thermocatalytic results of m-CN, $CsPbBr_3$ and m-CN@$CsPbBr_3$ samples under the temperature of 200 ^{o}C.

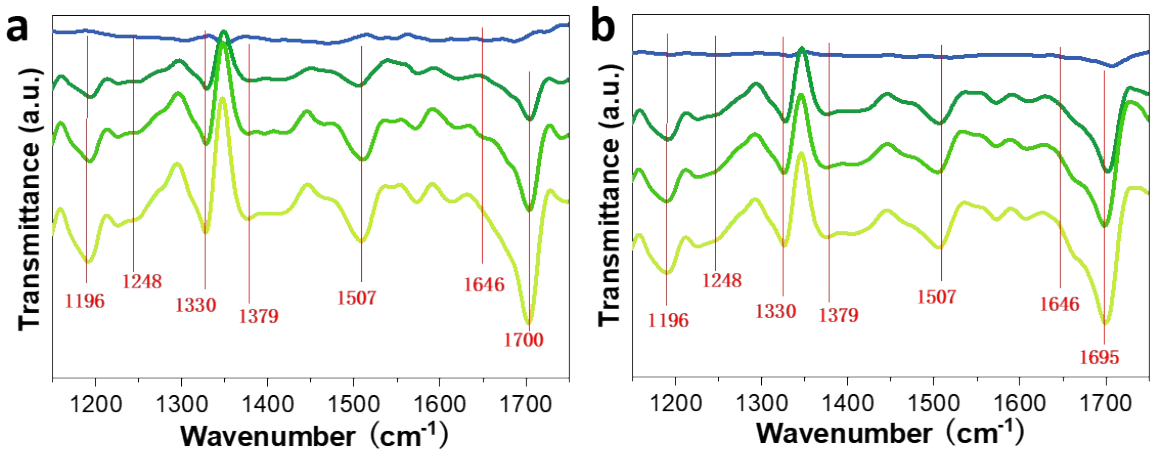

Figure S33. In situ FTIR results of bare $CsPbBr_3$ under (a) thermocatalytic and (b) photo-thermocatalytic conditions.

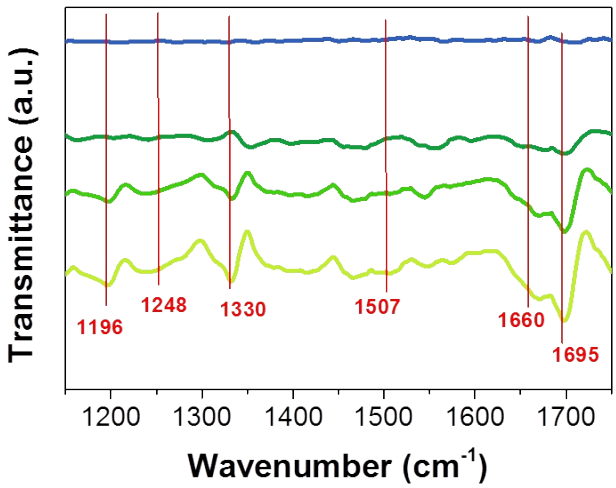

Figure S34. In situ FTIR results of bare m-CN under photo-thermocatalytic condition.

References

[1] J. Sheng, Y. He, J. Li, C. Yuan, H. Huang, S. Wang, Y. Sun, Z. Wang, F. Dong, *ACS Nano* 2020, **14**, 13103–13114.

[2] Z.-C. Kong, J.-F. Liao, Y.-J. Dong, Y.-F. Xu, H.-Y. Chen, D.-B. Kuang, C.-Y. Su, *ACS Energy Lett*. 2018, **3**, 2656–2662.

[3] Y. Jiang, J.-F. Liao, Y.-F. Xu, H.-Y. Chen, X.-D. Wang, D.-B. Kuang, *J. Mater. Chem. A* 2019, **7**, 13762-13769.

[4] M. Ou, W. Tu, S. Yin, W. Xing, S. Wu, H. Wang, S. Wan, Q. Zhong, R. Xu, *Angew. Chem., Int. Ed*. 2018, **57**, 13570.

[5] P. Li, S. Ouyang, G. Xi, T. Kako, J. Ye, *J. Phys. Chem. C* 2012, 116, **14**, 7621–7628.

[6] Y. F. Xu, M. Z. Yang, B. X. Chen, X. D. Wang, H. Y. Chen, D. B. Kuang, C. Y. Su, *J. Am. Chem. Soc*. 2017, **139**, 5660–5663.

[7] Y.-F. Xu, X.-D. Wang, J.-F. Liao, B.-X. Chen, H.-Y. Chen, D.-B. Kuang, *Adv. Mater. Interfaces* 2018, **5**, 1801015.

[8] L. Zhou, Y. F. Xu, B. X. Chen, D. B. Kuang, C. Y. Su, *Small* 2018, **14**, e1703762.

[9] F. Xu, K. Meng, B. Cheng, S. Wang, J. Xu, J. Yu, *Nat. Commun*. 2020, **11**, 4613.

[10] F. Sastre, A. Corma, H. García, *J. Am. Chem. Soc*. 2012, **134**, 14137–14141.

[11] Y. Jiang, J.-F. Liao, H.-Y. Chen, H.-H. Zhang, J.-Y. Li, X.-D. Wang, D.-B. Kuang, *Chem* 2020, **6**, 766-780.

[12] Y. Zhao, Y. Wei, X. Wu, H. Zheng, Z. Zhao, J. Liu, J. Li, *Appl. Catal., B* 2018, **226**, 360-372.

[13] M. Xing, Y. Zhou, C. Dong, L. Cai, L. Zeng, B. Shen, L. Pan, C. Dong, Y. Chai, J. Zhang, Y. Yin, *Nano Lett.* 2018, **18**, 3384–3390.